REPORT DOCUMENTATION PAGE

Form Approved
OMB No. 0704-0188

Public reporting burden for this collection of information is estimated to average 1 hour per response, including the time for reviewing instructions, searching existing data sources, gathering and maintaining the data needed, and completing and reviewing this collection of information. Send comments regarding this burden estimate or any other aspect of this collection of information, including suggestions for reducing this burden to Department of Defense, Washington Headquarters Services, Directorate for Information Operations and Reports (0704-0188), 1215 Jefferson Davis Highway, Suite 1204, Arlington, VA 22202-4302. Respondents should be aware that notwithstanding any other provision of law, no person shall be subject to any penalty for failing to comply with a collection of information if it does not display a currently valid OMB control number. **PLEASE DO NOT RETURN YOUR FORM TO THE ABOVE ADDRESS.**

1. REPORT DATE *(DD-MM-YYYY)*	**2. REPORT TYPE**	**3. DATES COVERED** *(From - To)*
December 2012	Journal Article	December 2012-December 2012

4. TITLE AND SUBTITLE
Comparison of Numerical and Experimental Time-Resolved Near-Field Hall Thruster Plasma Properties

5a. CONTRACT NUMBER
In-House

5b. GRANT NUMBER

5c. PROGRAM ELEMENT NUMBER

6. AUTHOR(S)

Ashley E. Gonzales, Justin W. Koo, and William A. Hargus Jr.

5d. PROJECT NUMBER

5e. TASK NUMBER

5f. WORK UNIT NUMBER
Q0AZ

7. PERFORMING ORGANIZATION NAME(S) AND ADDRESS(ES)

Air Force Research Laboratory (AFMC)
AFRL/RQRS
1 Ara Drive.
Edwards AFB, CA, 93524-7013

8. PERFORMING ORGANIZATION REPORT NO.

9. SPONSORING / MONITORING AGENCY NAME(S) AND ADDRESS(ES)

Air Force Research Laboratory (AFMC)
AFRL/RQR
5 Pollux Dr.
Edwards AFB, CA, 93524-7048

10. SPONSOR/MONITOR'S ACRONYM(S)

11. SPONSOR/MONITOR'S REPORT NUMBER(S)
AFRL-RQ-ED-JA-2012-473

12. DISTRIBUTION / AVAILABILITY STATEMENT
Approved for public release; distribution unlimited

13. SUPPLEMENTARY NOTES
Journal article published in the IEEE Transaction on Plasma Science, Vol. #42, Issue #3, March 2014.
PA Case Number: #13028; Clearance Date: 30 Jan 13.
© 2014 IEEE
The U.S. Government is joint author of the work and has the right to use, modify, reproduce, release, perform, display, or disclose the work.

14. ABSTRACT

Breathing mode oscillations of a xenon 600 W Hall effect thruster have been studied using temporally resolved experimental data and numerical modeling. Fluctuations in xenon neutral near infrared (810–835 nm) emission in the near field thruster plume have been measured at 1-μs resolution using a high speed, phase-matched intensified charge coupled device. Oscillations in electron temperature, 3–9 eV, have been inferred using a collisional-radiative model and a two-line ratio method. The time-resolved emission and electron temperature measurements are then used to assess the accuracy of the numerical model HPHall. Although simulations were able to accurately predict the time averaged thruster behavior, the model greatly under predicts the magnitude of the oscillations. General phase trends between the discharge current and emission as well as electron temperature are consistent with observations, suggesting that the model is capable of capturing some of the oscillatory behavior despite the dampening of the oscillations.

15. SUBJECT TERMS

16. SECURITY CLASSIFICATION OF:			**17. LIMITATION OF ABSTRACT**	**18. NUMBER OF PAGES**	**19a. NAME OF RESPONSIBLE PERSON**
					William Hargus
a. REPORT	**b. ABSTRACT**	**c. THIS PAGE**	SAR	8	**19b. TELEPHONE NO** *(include area code)*
Unclassified	**Unclassified**	**Unclassified**			**661-275-6799**

Standard Form 298 (Rev. 8-98)
Prescribed by ANSI Std. 239.18

Comparison of Numerical and Experimental Time-Resolved Near-Field Hall Thruster Plasma Properties

Ashley E. Gonzales, Justin W. Koo, and William A. Hargus, Jr.

***Abstract*— Breathing mode oscillations of a xenon 600 W Hall effect thruster have been studied using temporally resolved experimental data and numerical modeling. Fluctuations in xenon neutral near infrared (810–835 nm) emission in the near field thruster plume have been measured at 1-μs resolution using a high speed, phase-matched intensified charge coupled device. Oscillations in electron temperature, 3–9 eV, have been inferred using a collisional-radiative model and a two-line ratio method. The time-resolved emission and electron temperature measurements are then used to assess the accuracy of the numerical model HPHall. Although simulations were able to accurately predict the time averaged thruster behavior, the model greatly under predicts the magnitude of the oscillations. General phase trends between the discharge current and emission as well as electron temperature are consistent with observations, suggesting that the model is capable of capturing some of the oscillatory behavior despite the dampening of the oscillations.**

***Index Terms*— Breathing mode, hall thruster, HPHall, plume emission.**

I. Introduction

HALL thrusters are a plasma propulsion technology widely used due to their low thrust, high specific impulse operation. With increasing demand for these thrusters to perform a wide range of missions, there is a need to move away from the costly experiment-based thruster development to a more efficient numerical modeling-based approach. Current efforts have focused on improvements to the numerical model HPHall. The HPHall is a radial-axial hybrid particle-in-cell (PIC) model, which is based on a fluid treatment of electrons and a PIC treatment of ions and neutrals as first developed by Fife [1]. Although HPHall has been moderately successful at predicting overall thruster performance [1]–[7], verification is needed to determine its ability to accurately model the more complex features of thruster operation. Of particular interest is the low frequency (10–50 kHz) fluctuation in discharge current, often referred to in literature as the breathing mode [8], [9]. The fluctuations are believed to be due to a periodic cycling of the neutral and plasma density in the exhaust region and are thought to have a strong influence on electron transport.

Although simulations have been able to qualitatively reproduce the plasma oscillations observed experimentally in the breathing mode [1]–[4], the lack of time-resolved data has made it difficult to validate. Recent efforts have been made to develop time-resolved techniques on the breathing mode timescale (30 μs).

Recently, time-resolved probe measurements of the far plume using retarding field electrostatic analyzers as well as Langmuir and emissive probes have provided electron density, electron temperature, plasma potential, and ion energy measurements on the 1–10-μs timescales [10]–[13]. However, probe measurements are limited to the far-field due to their interference with the plume, making them typically outside HPHall's computational domain. Optical measurements are an attractive alternative, capable of nonintrusively characterizing the near field, with resolution on the ns timescale. These measurements are mainly limited by signal-to-noise ratio (SNR) and the speed of the optical components. Time-resolved emission has been studied using 2-D CCD images of the plume as well as interior channel measurements using a thruster integrated fiber array [10], [14]. Additionally, time-resolved laser-induced fluorescence (LIF) techniques have been developed, which nonintrusively measure the ion energy distribution function [15], [16].

In this paper, time-resolved emission measurements of the near field of a 600-W Hall thruster are presented. Breathing mode oscillations in xenon neutral near infrared (NIR) emission are measured with a 1-μs resolution using a fiber-coupled spectrometer and high speed, phase-locked intensified charge coupled device (ICCD). Oscillations in electron temperature are inferred using a collisional-radiative model (CRM) [17]. The resulting characterization of the breathing mode cycle is then used to assess the temporal fidelity of the numerical model HPHall.

II. Experimental Measurement

A. Test Facility and Thruster

The measurements reported here were performed in vacuum Chamber 1 at the Air Force Research Laboratory at Edwards Air Force Base. This vacuum facility consists of a 2.4-m diameter, 4.1-m long cylindrical, nonmagnetic stainless steel vacuum chamber with two liquid nitrogen baffled (76 K),

Manuscript received February 11, 2013; revised September 27, 2013; accepted January 7, 2014. Date of publication February 3, 2014; date of current version March 6, 2014. Distribution A: Approved for public Release; distribution unlimited. PA Clearance Number 13028.

The authors are with the U.S. Air Force Research Laboratory, Edwards AFB, CA 93524 USA (e-mail: ashley.gonzales.4@us.af.mil; justin.koo@edwards.af.mil; william.hargus@edwards.af.mil).

Color versions of one or more of the figures in this paper are available online at http://ieeexplore.ieee.org.

Digital Object Identifier 10.1109/TPS.2014.2301038

0093-3813 © 2014 IEEE. Personal use is permitted, but republication/redistribution requires IEEE permission.
See http://www.ieee.org/publications_standards/publications/rights/index.html for more information.

TABLE I
BHT-600 HALL THRUSTER AT NOMINAL XENON OPERATING CONDITIONS AND PERFORMANCE [21]

Parameter	Value
Anode Flow Rate	2.45 mg/s
Cathode Flow Rate	0.197 mg/s
Anode Potential	300 V
Anode Current	2.05 A
Magnetic Current (inner coils)	2.0 A
Magnetic Current (outer coils)	2.0 A
Thrust	39 mN
Specific Impulse	1530 s
Propulsive Efficiency	49%

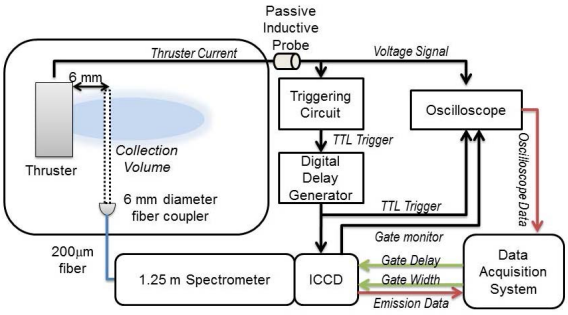

Fig. 1. Optical system used to measure thruster emission using a 1.25-m Horiba spectrometer with attached Andor ICCD. Emission measurements are triggered using a custom triggering circuit to synchronize measurements to current oscillations. Full breathing mode cycle is characterized by varying the delay between the trigger and ICCD gating.

1.2-m flanged gaseous helium two stage cryogenic (15 K) vacuum pumps capable of pumping speeds of 48 500 L/s on xenon. A cold cathode gauge is used to determine a chamber background pressure of approximately 4×10^{-6} torr (corrected for xenon) during thruster operation.

The Hall thruster used in this paper is a 600 W BHT-600 with a 3.2-mm hollow cathode manufactured by the Busek Company (Natick, MA). This thruster has been studied previously using both electrostatic probes and various optical diagnostics [17]–[20]. The BHT-600 has an acceleration channel outer radius of 32 mm, inner radius of 24 mm, and depth of 10 mm. The magnetic field is produced by four outer coils, and one inner magnetic coil. The outer and inner coil currents are independently adjustable for optimization of the field strength. The nominal conditions and performance of the BHT-600, as provided by the Busek Company, are shown in Table I [21]. Nominal conditions of the thruster produce breathing mode oscillations with a very narrow frequency (38 ± 0.3 kHz). These conditions allow for the phase-matched averaging technique described in subsequent sections.

B. Emission Measurements

Plume emission measurements of the near field were collected using the optical system shown schematically in Fig. 1. Emission was collected at a single location 6-mm downstream of the thruster exit plane using a reflective fiber optic beam coupler with a 6-mm diameter and greater than 97.5% reflectance in the 450 nm–2 μm range. The emission was then transmitted through the chamber using a fiber optic feed through and a 200-μm fiber with a numerical aperture of 0.22 and low attenuation in the NIR. A fiber optic adapter was used to couple with a Horiba 1250M Series II spectrometer with a 1.25-m focal length (f/9), 300-G/mm classically ruled diffraction grating, blazed at 500 nm, and a dispersion of 2.6 nm/mm. The spectrometer entrance slit was fixed at 200 μm to increase throughput for greater signal strength.

The emission spectrum is detected using a cooled Andor iStar ICCD with 1024 $\times$ 1024 pixels (13 μm $\times$ 13 μm) capable of dark currents as low as 0.065 e^-/pix/s. The camera intensifier system acts as a fast solid-state shutter capable of gating on 1-ns time scales. Gating is controlled by transistor-transistor logic (TTL) input and user defined gate delay and gate width. The individually gated shots are accumulated over the length of the exposure and recorded using the National Instruments LabView PC-based data acquisition system.

Emission measurements were background subtracted and wavelength calibrated using a standard xenon spectral lamp. A relative spectral response (RSR) calibration was applied to correct for any wavelength dependence of emission detection due to the transmission losses introduced by the optical components. The RSR was determined using a National Institute of Standards and Technology traceable 200-W tungsten filament standard of spectral irradiance and comparing the measured gray body emission with the ideal spectral response.

C. Timing and Triggering Circuit

Time resolved measurements were achieved using a phase-locked triggering system, which synchronized ICCD gating with 1 μs portions of the breathing mode cycle. Temporal resolution was achieved by varying cycle phase of the gated portion. Adequate SNR was achieved by integrating phase-locked shots over a 0.5-s exposure.

A custom trigger circuit and digital delay generator (DDG) were used to process the discharge current signal into an ICCD trigger compatible TTL output. Thruster current oscillations were measured using a passive inductive probe, which acts as a bandpass filter (3-dB points of 120 Hz and 20 MHz with $< 1^\circ$ phase shift at frequencies between 1 and 100 kHz). This low-level voltage signal was then passed through a low-pass filter and subsequently differentiated, so that the zero crossings of the differentiated signal corresponded to the maximum and minimum in the thruster anode current signal. A high-speed comparator was then used as a zero crossing detector, which produced a TTL signal synchronized with the minimum of the discharge current signal. The TTL was then passed through a DDG to output a clean TTL trigger to the ICCD. Characterization of the entire cycle was then achieved by varying the DDG delay between the synchronized TTL input and the ICCD trigger output.

To ensure gating is correctly synchronized to the desired portion of the signal, a 1-GS/s oscilloscope is used to monitor the thruster discharge current, the TTL trigger, and the ICCD gate monitor output. A sample oscilloscope trace is shown

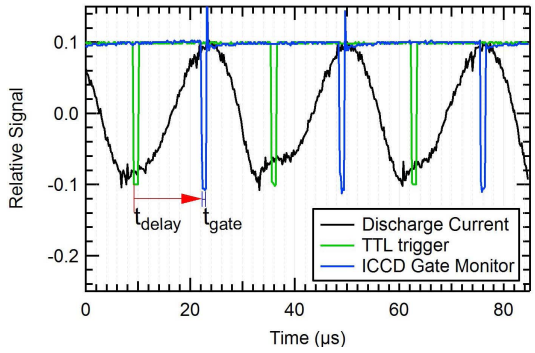

Fig. 2. Sample oscilloscope trace. ICCD settings: 1-μs gate pulsewidth, 13-μs gate delay. Note: only 80 μs of the 0.5-s exposure is shown.

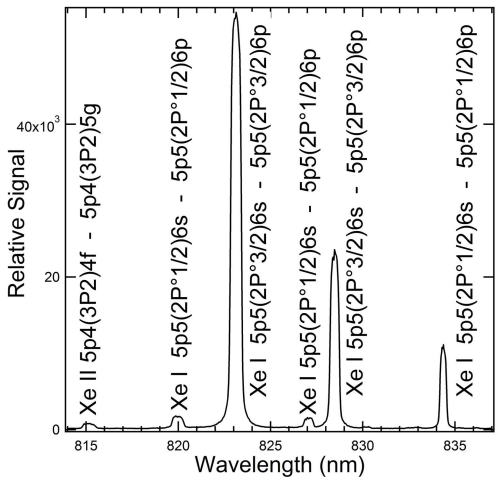

Fig. 3. Sample emission spectrum of a BHT-600 at nominal operating conditions. Measurement taken near peak of discharge current oscillation with 1-μs gated shots over a 0.5-s exposure (19 000 cycles).

in Fig. 2. The discharge current is shown to oscillate at 38 $\pm$ 0.3 kHz over a mean value of 2.05 A. The sample trace is shown with ICCD settings of 1-μs pulsewidth and 13-μs gate delay. Upon receiving the input trigger and waiting the specified delay time, the ICCD is gated for the duration of the pulsewidth. Signal is accumulated over several gating cycles until the end of the exposure. Measurement of the full breathing mode cycle is achieved by varying the gate delay from 0 to 26 μs. The 2 μs delay between the minimum of the current signal and the trigger is caused by the delays added by the active circuit components and was found to be consistent in all measurements. Additional delay added by ICCD electronics was found to be in the order of nanoseconds, and are assumed negligible. Time zero shown in subsequent figures will be defined at the fall of the TTL trigger, corresponding to an input gate delay of zero. A $\pm$0.2 μs uncertainty in the temporal resolution will be used based on the half width half max (HWHM) of the current FFT.

D. Electron Temperature Measurements

Electron temperature measurements were achieved using emission lines with a known dependence on electron temperature. Emission measurements were taken in the 810–840 nm NIR region to include the 823, 828, and 834 nm neutral xenon lines. A collisional-radiative model (CRM) based on the model developed by Karabadzhak *et al.* [22] is used to determine the electron temperature dependence of the I_{823}/I_{828} and I_{834}/I_{828} line ratios. The Karabadzhak, Chiu and Dressier (KCD) model uses empirical excitation cross sections [23], [24] and probability statistics to model Xe I metastable populations. The line intensity per unit volume can be approximated by

$$J^{\lambda}_{\mathrm{Xe\,I}} = \frac{\mathrm{hc}}{4\pi\lambda}(N_0 N_e) B^{\lambda} C^{\lambda} \tag{1}$$

where N_i are the species number densities, and the rate term B^{λ} can be determined using

$$B^{\lambda} = k^{\lambda}_{e0} + \alpha k^{\lambda}_{10} + \frac{1-\alpha}{2} k^{\lambda}_{20} \tag{2}$$

where $\alpha = N_1/N_e$, and k^{λ}_{ij} is the excitation rate coefficient at wavelength λ for the $i-j$ species collision. The metastable correction term C^{λ} is approximated using the upper 2 p_i level degeneracy and branching probabilities [22].

Errors with this temperature method are due to two main factors. First, experimental uncertainties in the emission collection will propagate through to uncertainties in electron temperature. Most significant of these is the uncertainties in line fit, which can lead to line ratio uncertainties as high as 5% for low SNR line profiles. This results in a 1 eV uncertainty for the I_{823}/I_{828} ratio method and a 2 eV uncertainty for the I_{834}/I_{828} ratio method. Second, there are some uncertainties inherent to the KCD model assumptions, which are not quantified. These uncertainties will be most significant for the I_{823} line, which relies on the metastable approximation.

The I_{823}/I_{828} ratio method relies on the ratio of the two strongest of the lines, reducing the temperature uncertainty due to uncertainties in line fit associated with low SNR. However, this method relies on the metastable approximations for I_{823} line, which is not reflected in the temperature uncertainty. The I_{834}/I_{828} ratio method is more accurately modeled, but the lower intensity of the I_{834} leads to issues with SNR and higher line fit uncertainty. Therefore the I_{834}/I_{828} ratio method should not be used in conditions with low electron temperature or low emission signal.

III. Experimental Result

A. Emission Measurements

Emission measurements were taken 6-mm downstream of the thruster exit with a temporal resolution of 1 μs in the NIR (810–835 nm). The cooled ICCD achieved a high SNR $>$24 dB for most of the cases. Emission measurements near the minimum of the discharge current were difficult due to the low signal (SNR = 1.9 dB). A sample emission spectrum is shown in Fig. 3. The majority of the measured lines in this wavelength region are strong neutral lines. The emission from the metastable linked 823-nm line is the strongest of the three lines. The metastable state allows for excited neutrals with long lifetimes, which can then be easily reexcited producing strong emission lines. Additional neutral Xe lines are observed at 820 and 827 nm, but their low signal in proximity to

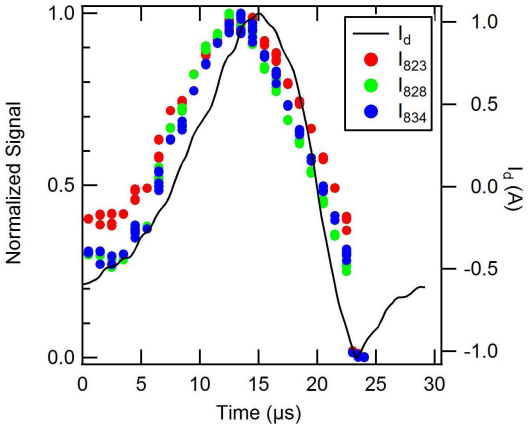

Fig. 4. Normalized Xe I line intensities in comparison with discharge current. Measurements taken 6-mm downstream of thruster exit plane at nominal operating conditions. Line intensities at the end of the cycle are undetermined due to low SNR.

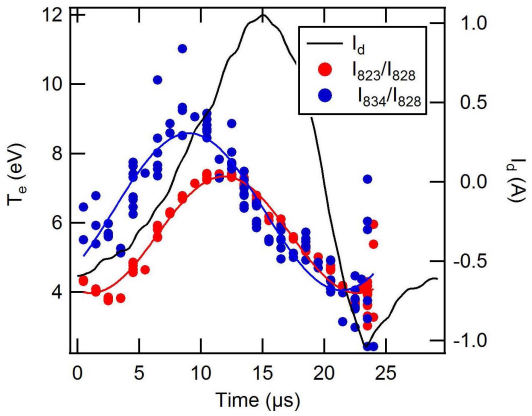

Fig. 5. Electron temperature fluctuations 6-mm downstream of BHT-600 thruster exit plane at nominal operating conditions using the KCD model a two-line emission method.

the stronger lines makes them difficult to use for diagnostic purposes. The three strongest lines (823, 828, and 834 nm) are the focus of this paper.

The peak value normalized line intensities are shown in Fig. 4 with a representative current trace. There is a strong correlation between the peak of the discharge current and the peak of the Xe neutral emission, as observed in [10] and [14]. A 2 μs delay is shown between the peak of the normalized intensity and the peak in the discharge current. Based on the delay and travel distance to the anode, an 8 ± 1-km/s average axial velocity can be inferred. Delays measured differ from previous measurements by Bouchoule *et al.* due to differing thruster geometry, but a comparable 5 km/s average axial velocity can be inferred near the thruster exit using a similar method. A significant drop in emission signal is observed after 23 μs, near the minimum of the discharge current. The low signal in this portion of the cycle increased the uncertainty in line intensity measurements, especially for the lowest intensity line at 834 nm.

B. Electron Temperature

Electron temperatures are determined using I_{823}/I_{828} and I_{834}/I_{828} line intensity ratios and the two-line method of the KCD model. The resulting electron temperatures are shown in Fig. 5. The two methods are in general agreement, with electron temperatures fluctuating between 3 and 10 eV, -4.5 ± 1.5 μs out of phase with discharge current oscillations. The I_{823}/I_{828} ratio method results in an electron temperature of 5.6 ± 1.0 eV oscillating at ± 1.7 eV approximately -3 μs out of phase with discharge current. The I_{834}/I_{828} ratio method results in an electron temperature of 6.3 ± 2.0 eV oscillating at ± 2.3 eV, approximately -6 μs out of phase with discharge current.

Lower temperature measurements of the I_{823}/I_{828} method may be due higher order Xe I and Xe II lines being integrated into the I_{823} signal, causing a higher ratio and lower inferred temperature. Future measurements will look into increasing the spectral resolution to better characterize the line feature. Higher scatter in the I_{834}/I_{828} versus the I_{823}/I_{828} ratio method is due to the I_{834}/I_{828} method's higher sensitivity to uncertainty in line ratio. Low signal at the end of the cycle (>22 μs) led to higher uncertainties with the integrated line intensity for all three lines, and therefore resulted in a higher uncertainty for both temperature methods.

The $37\% \pm 15\%$ oscillations in electron temperature are comparable with the 20%–30% observed in far field probe measurements [11]–[13]. However, phase (relative to I_d) vary across studies. Recently, it has been shown that the magnitude and phase delay of the electron temperature oscillations may vary immensely depending on breathing mode conditions [11]. Future measurements at similar breathing mode conditions are needed for further comparison of probe and optical measurements.

IV. Numerical Modeling

HPHall simulations were run at nominal operating conditions with a time step of 0.25 μs over a 2-ms time period. A sensitivity analysis was performed to determine the model's dependence on input conditions, particularly sensitivity to electron mobility profile. HPHall uses an effective mobility profile to account for the anomalous electron mobility not described by classical theory. The effective mobility can be described by

$$\mu_{\perp \text{eff}} = \mu_{\perp \text{classical}} + \mu_{\text{Bohm}} \tag{3}$$

$$\mu_{\text{Bohm}} = \frac{K_B}{16}\frac{1}{B} \tag{4}$$

where K_B is Bohm fitting parameter, typically adjusted between 0 and 1. The $K_B/16$ term is referred to as the inverse Hall parameter. HPHall assumes an axially varying inverse Hall parameter, similar to that measured by Meezan *et al.* [25].

To determine the model's sensitivity electron mobility profiles, simulations were run with varying inverse Hall parameter profiles, as shown in Fig. 6. A representative test case was chosen based on the comparison with experimentally observed performance parameters (T, I_{SP}, f_{BM}). The results are then used in conjunction with the KCD CRM to predict emission fluctuations. Simulated oscillations in emission intensity and electron temperature are compared with the experimental data

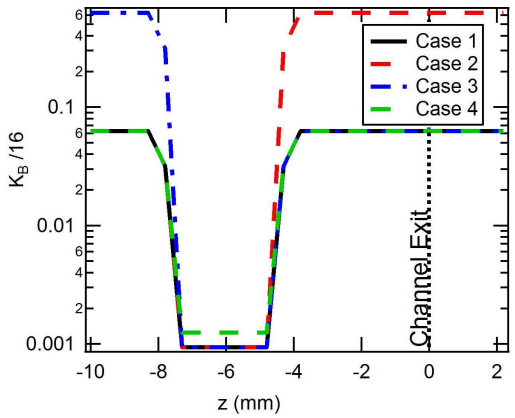

Fig. 6. Inverse Hall parameter profiles used in simulation cases.

to assess the model's ability to characterize the breathing mode behavior.

V. Numerical Modeling Result

A. HPHall Simulation Results

A summary of the measured and simulated thruster performance is shown in Table II. Measured thrust and I_{SP} performance metrics are based on published Busek values [18]. Electron temperature predictions from HPHall are based on an electron density weighted average of T_e evaluated in the experimental emission collection volume. Oscillation magnitudes are estimated using a ratio of the standard deviation to the mean value.

Although the model was successful in predicting the overall thruster performance within 10% for all four cases, all cases had difficulty accurately modeling breathing mode behavior. Most of the cases were able to predict average discharge current within 10%, but all were significantly under the 32% oscillations measured in discharge current. All simulations predicted higher than observed electron temperatures with significantly lower oscillation magnitudes, 2%–6% versus 37% ± 15% observed.

Differences in the four cases can be observed in the breathing mode frequency, f_{BM}, indicating that breathing mode predictions are highly sensitive to choice of inverse Hall parameter profile. Changes in frequency appear to be nonlinear, suggesting a complex relationship between the electron mobility and breathing mode frequency. Further analysis in this paper will focus on Case 1, based on the compatibility of measured and Case 1 predicted values.

Oscillations in plasma properties were sampled at four axial locations: 1) channel near anode (−5 mm); 2) channel exit (0 mm); 3) near plume (6 mm); and 4) far plume (10 mm). The cross correlation was determined by evaluating the correlation coefficient R between the discharge current and the plasma property, while varying the delay (τ) to the plasma property as defined by

$$R_{I_d,x}(\tau) = \frac{\sum(I_d(t) - \bar{I}_d)(X(t+\tau) - \bar{X})}{\sqrt{\sum(I_d(t) - \bar{I}_d)^2 \sum(X(t+\tau) - \bar{X})^2}}. \quad (5)$$

TABLE II
Comparison of HPHall Predicted Performance

	Units	Measured	HPHall			
			Case 1	Case 2	Case 3	Case 4
T	mN	39	38	38	38	41
I_{SP}	s	1530	1530	1510	1530	1660
f_{BM}	kHz	38	34± 5	54± 5	31± 5	22 ± 5
I_d	A	2.05	2.18	2.21	2.2	3.64
$\frac{\tilde{I}_d}{I_d}$		32%	7%	11%	7%	6%
T_e	eV	6.3 ± 2.0	12.4	10.4	12.7	25.8
$\frac{\tilde{T}_e}{T_e}$		37 ± 15 %	4%	6%	4%	2%

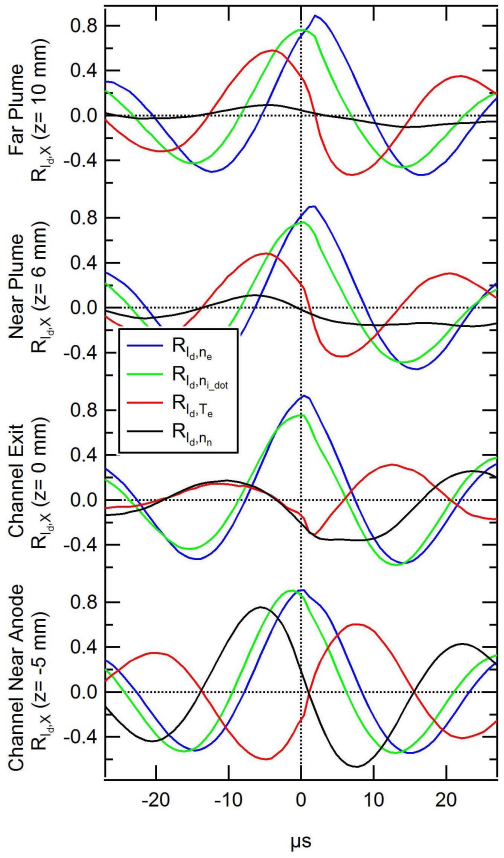

Fig. 7. HPHall Case 1 cross correlations of plasma properties with discharge current.

Cross-correlations between the plasma properties with the discharge current were evaluated at each axial location and are shown in Fig. 7. The τ, which corresponds to the peak in $R_{I_d,x}$ is used to determine the delay and phase shift between the discharge current and plasma property.

A summary of the simulation is shown in Table III. The magnitudes of the oscillations are estimated using ratio of the standard deviation to the mean value ($\tilde{x}/\bar{x}$). An uncertainty of ±5 kHz for the breathing mode frequency is based on the HWHM of the spectrum peak. Delays between the discharge current and the plasma property were determined using the peak of the cross correlation. An uncertainty of ±1 μs

TABLE III
SUMMARY OF HPHALL CASE 1 PREDICTED PLASMA PROPERTY FLUCTUATIONS

	z (mm)	$\bar{x}$	$\tilde{x}/\bar{x}$ (%)	f_{BM} (kHz)	τ_{delay} (μs)	$\phi_{I_d,x}$ (deg)	$R_{I_d,x}$
I_d	–	2.1 A	7	34	–	–	1.00
n_0	-5	9.4 10^{18} m^{-3}	4	33	-5.6	-68	0.75
	0	2.2 10^{18} m^{-3}	5	33	-4.0	-76	0.26
	6	5.3 10^{17} m^{-3}	7	28	-6.4	-65	0.11
	10	3.3 10^{17} m^{-3}	7	33	-4.9	-59	0.09
n_i	-5	1.1 10^{24} m^{-3}/s	8	33	-1.1	-14	0.90
	0	1.7 10^{23} m^{-3}/s	9	34	-0.4	-5	0.75
	6	1.8 10^{22} m^{-3}/s	12	34	0.4	5	0.76
	10	5.3 10^{21} m^{-3}/s	13	33	0.4	5	0.76
n_e	-5	1.1 10^{18} m^{-3}	7	34	0.4	5	0.91
	0	6.3 10^{17} m^{-3}	8	34	0.4	5	0.93
	6	3.4 10^{17} m^{-3}	8	34	1.9	23	0.90
	10	2.4 10^{17} m^{-3}	9	33	1.9	23	0.89
T_e	-5	27.3 eV	2	34	7.9	96	0.60
	0	22.8 eV	2	34	12.4	153	0.31
	6	16.4 eV	4	34	-4.9	-59	0.48
	10	12.4 eV	5	34	-4.1	-50	0.58

is based on the accuracy of the cross correlation method. Phase shift, $\phi_{I_d,x}$, is determined as a ratio of the delay to the oscillation period, expressed in degrees. Low confidence values, correlation coefficient ($R < 0.30$), are shown in blue.

Oscillations in electron density and ionization rate were found to be relatively in-phase, $|\phi| < 23°$, with discharge current. Neutral densities were found to be out of phase with discharge current oscillations. This is consistent with the ionization bursts associated with breathing mode theory. Electron temperatures simulations at $z = 6$ mm were found to be out of phase with discharge current, $\phi = -59°$. Although simulations significantly underpredict the magnitude of the electron temperature oscillations, phase behavior is comparable with phase delays observed experimentally between the discharge current and electron temperature ($\phi = -69°$).

B. HPHall-KCD Simulation Results

Mean normalized oscillations of emission intensity (J_λ) and discharge current (I_d) are shown in Fig. 8 for $\lambda = 823$ nm. Also shown are oscillations in electron and neutral populations (N_e, N_0), the rate term (B^λ), and the metastable correction term (C^λ), where $J_\lambda \sim N_e N_0 B^\lambda C^\lambda$. Oscillations in emission intensity are shown to be primarily due to strong oscillations in electron density with additional contributions from more subtle oscillations in B^λ. Oscillations in B^λ are due primarily to oscillations in the dominant $k_{e0}(T_e)$ term.

Cross-correlations analysis shows a strong correlation between the discharge current and emission intensity, electron density, and the rate term. A weaker negative correlation is observed between the discharge current and the metastable correction term, suggesting the metastable population varies inversely with discharge current. The slight phase delay ($\phi = 25°$) between the discharge current and emission intensity is inconsistent with measurements, where the peak in intensity occurs before the peak in discharge current ($\phi = -28°$).

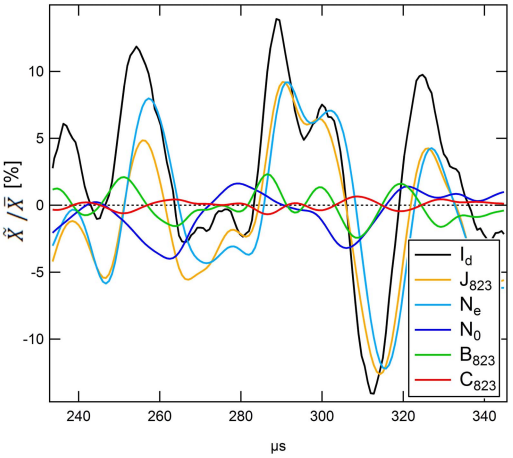

Fig. 8. Predicted oscillations using HPHall coupled with the KCD CRM, with emission intensity, $J_\lambda \sim N_e N_0 B^\lambda C^\lambda$.

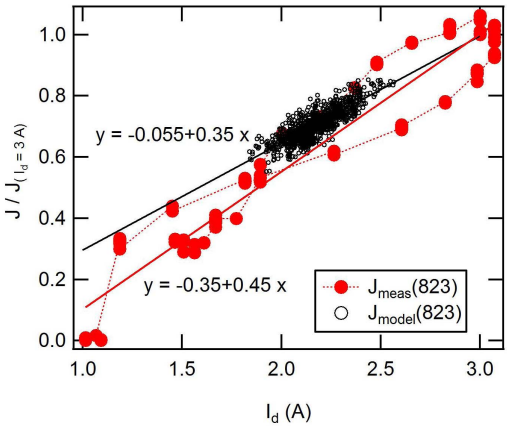

Fig. 9. Comparison of measured emission intensity, J^{823}_{meas}, and HPHall-KCD predicted emission intensity, J^{823}_{model}.

A comparison of the numerical (HPHall-KCD) and experimental emission data, normalized for $J_\lambda(I_d = 3$ A), is shown in Fig. 9. Measurements are shown for one breathing mode cycle due to the phase-matched experimental procedure, unlike numerical data which is shown over several cycles. Although simulations greatly under-predicted the magnitude of discharge current oscillations, the HPHall-KCD modeling was able to predict the positive correlation observed between the discharge current and emission intensity. The shape of the experimental curve suggests a nonlinear relationship between the discharge current and emission intensity, emphasizing the importance of cycle phase in future correlation studies.

VI. CONCLUSION

New time-resolved methods have been developed to gain understanding of the complex dynamics of the Hall thruster breathing mode. Time resolved (1 μs) emission measurements were taken of the near plume using a high speed, gated ICCD. The I_{823}/I_{828} and I_{834}/I_{828} line intensity ratios were used in conjunction with the KCD CRM to determine electron temperature. Electron temperatures in the near plume were found to fluctuate between 3 and 10 eV. A strong correlation

between the discharge current and electron temperature was observed with a significant phase shift ($\phi = -69°$) between the cycles.

Simulations were performed using HPHall and the KCD model. Results were compared with the experimental data to validate HPHall's breathing mode predictions. Although the model was able to correctly estimate the time averaged performance metrics, the model had difficultly capturing the more complex breathing mode oscillations. Differences in breathing mode frequency between the simulation cases emphasize the model's sensitivity to choice of inverse Hall parameter profile. General phase trends of the model are in agreement with the experimental data. However, the simulations greatly underpredict the magnitude of the oscillations. Additionally, the simulations predict higher than observed electron temperatures. Similar results were observed by Garrigues *et al.* who compared the numerical and experimental time-resolved LIF measurements. Although the model is able to capture the most probable velocity of the ion velocity distribution function, it underestimates the dispersion of the distribution by as much as a factor of four. It has been suggested that this is a result of the imposed time-independent Bohm mobility profile.

HPHall attempts to capture the turbulent mobility using an effective mobility with the addition of a fixed Bohm mobility term. The Bohm mobility profiles are selected through an iterative process designed to capture steady-state thruster behavior (including the discharge potential and current), but the fixed profiles fail to capture dynamic thruster behavior. In reality, the turbulent mobility is coupled with oscillating plasma dynamics and therefore some interplay is expected on the 10–100-kHz timescale between the plasma density and mobility profile. By imposing a fixed mobility, it is effectively damping the oscillations of the system, which in the case of current measurements, may also be producing the higher than observed electron temperatures. Future modeling work is needed to develop a dynamic mobility profile, which efficiently captures the coupling between the oscillatory thruster behavior and the effective mobility profile.

ACKNOWLEDGMENT

The authors would like to thank Dr. M. Holmes and P. Adkison for their assistance with development of the triggering system, as well as M. Nakles for his assistance with the experimental work.

REFERENCES

[1] J. M. Fife, "Modeling and electrostatic probe survey of Hall thrusters," Ph.D. dissertation, Dept. Aeronautics and Astronautics, Massachusetts Inst. Technol., Cambridge, MA, USA, 1998.

[2] F. I. Parra, E. Ahedo, J. M. Fife, and M. Martinez-Sanchez, "A two-dimensional hybrid model of the Hall thruster discharge," *J. Appl. Phys.*, vol. 100, no. 2, pp. 023304-1–023304-11, 2006.

[3] R. R. Hofer, I. Katz, I. G. Mikellides, and M. Gamero-Castano, "Heavy particle velocity and electron mobility modeling in hybrid-PIC Hall thruster simulations," in *Proc. 42nd AIAA/ASME/SAE/ASEE Joint Propuls. Conf. Exhibit.*, Jul. 2006, pp. 1–17.

[4] J. Barreilles, G. J. M. Hagelaar, L. Garrigues, C. Boniface, and J. P. Boef, "Critical assessment of a two-dimensional hybrid Hall thruster model: Comparisons with experiments," *Phys. Plasmas*, vol. 11, no. 6, p. 3035, 2004.

[5] J. W. Koo, "Hybrid PIC-MCC computational modeling of Hall thrusters," Ph.D. dissertation, Dept. Aerosp. Eng. Sci. Comput., Univ. Michigan, Ann Arbor, MI, USA, 2005.

[6] M. R. Nakles, L. Brieda, G. Reed, W. A. Hargus, and R. L. Spicer, "Experimental and numerical examination of the BHT-200 Hall thruster plume," in *Proc. 43rd AIAA/ASME/SAE/ASEE Joint Propuls. Conf.*, Jul. 2007, pp. 20–23.

[7] M. K. Scharfe, N. Gascon, and M. A. Cappelli, "Comparison of hybrid Hall thruster model to experimental measurements," *Phys. Plasmas*, vol. 13, no. 8, p. 083505, 2006.

[8] J. P. Boeuf and L. Garrigues, "Low frequency oscillations in a stationary plasma thruster," *J. Appl. Phys.*, vol. 84, no. 7, pp. 3541–3554, 1998.

[9] E. Y. Choueiri, "Plasma oscillations in Hall thrusters," *Phys. Plasmas*, vol. 8, no. 4, pp. 1411–1426, Apr. 2001.

[10] A. Bouchoule, C. Philippe-Kadlec, M. Prioul, F. Darnon, M. Lyszyk, L. Magne, *et al.*, "Transient phenomena in closed electron drift plasma thrusters: Insights obtained in a French cooperative program," *Plasma Sources Sci. Technol.*, vol. 10, no. 2, p. 364, 2001.

[11] K. Dannanmayer, P. Kudrna, M. Tichy, and S. Mazouffre, "Time-resolved measurement of plasma parameters in the far-field plume of a low-power Hall effect thruster," *Plasma Sources Sci. Technol.*, vol. 21, no. 5, p. 055020, 2012.

[12] R. B. Lobbia, "A time-resolved investigation of the Hall thruster breathing mode," Ph.D. dissertation, Dept. Aerosp. Eng., Univ. Michigan, Ann Arbor, MI, USA, 2010.

[13] R. B. Lobbia and A. D. Gallimore, "High-speed dual Langmuir probe," *Rev. Sci. Instrum.*, vol. 81, no. 7, p. 073503, 2010.

[14] D. Liu, R. E. Huffman, R. D. Branam, and W. A. Hargus, "Ultra-high speed imaging of Hall thruster discharge oscillations with krypton propellant," *IEEE Trans. Plasma Sci.*, vol. 39, no. 11, pp. 2926–2927, Nov. 2011.

[15] L. Garrigues, S. Mazouffre, and G. Bourgeois, "Computed versus measured ion velocity distribution functions in a Hall effect thruster," *J. Appl. Phys.*, vol. 111, no. 11, pp. 113301-1–113301-8, 2012.

[16] N. MacDonald, M. Cappelli, and W. Hargus, "Time-synchronized continuous wave laser-induced fluorescence on an oscillatory xenon discharge," *Rev. Sci. Instrum.*, vol. 83, no. 11, p. 113506, 2012.

[17] A. E. Gonzales, W. A. Hargus, and M. R. Nakles, "Non-intrusive, time-resolved Hall thruster near-field electron temperature measurements." in *Proc. 47th AIAA/ASME/SAE/ASEE Joint Propuls. Conf. Exhibit.*, 2011, pp. 1–13.

[18] M. R. Nakles, R. R. Barry, C. W. Larson, and W. A. Hargus, "A plume comparison of xenon and krypton propellant on a 600 W Hall thruster," in *Proc. 31st Int. Electr. Propuls. Conf.*, 2009, pp. 1–3.

[19] J. M. Ekholm, W. A. Hargus, W. Larson, M. R. Nakles, G. Reed, and C. S. Niemela, "Plume characteristics of the Busek 600 W Hall thruster," in *Proc. 42nd AIAA/ASME/SAE/ASEE Joint Propuls. Conf.*, 2006, pp. 1–10.

[20] M. R. Nakles and W. A. Hargus, "Background pressure effects on internal and near-field ion velocity distribution of the BHT-600 Hall thruster," in *Proc. 44th AIAA/ASME/SAE/ASEE Joint Propuls. Conf.*, 2008, pp. 1–9.

[21] Busek Co. Natick, MA, USA. (2005). *Busek Low Power Hall Thrusters Data Sheet* [Online]. Available: http://www.busek.com/index_htm_files/70008510.pdf

[22] G. F. Karabadzhak, Y. Chiu, and R. A. Dressler, "Passive optical diagnostic of Xe propelled Hall thrusters. II. Collisional-radiative model," *J. Appl. Phys.*, vol. 99, no. 11, pp. 113305-1–113305-12, 2006.

[23] Y. Chiu, B. L. Austin, S. Williams, R. A. Dressler, and G. F. Karabadzhak, "Passive optical diagnostic of Xe-propelled Hall thrusters. I. Emission cross sections," *J. Appl. Phys.*, vol. 99, no. 11, pp. 113304-1–113304-11, 2006.

[24] J. D. Sommerville, "Emission cross sections for neutral xenon impacted by Xe_+ and Xe_{2+}," Ph.D. dissertation, Dept. Sci. Mech. Eng., Michigan Technol. Univ., Houghton, MI, USA, 2006.

[25] N. B. Meezan, "Electron transport in a coaxial Hall discharge," Ph.D. dissertation, World Acad. Res. Sci. Eng., Stanford Univ., Stanford, CA, USA, 2002.

Authors' photographs and biographies not available at the time of publication.